Inorganic Chemistry

Article

pubs.acs.org/IC

$VSb(SeO_3)_4$, First Selenite Containing V^{3+} Cation: Synthesis, Structure, Characterization, Magnetic Properties, and Calculations

Yiseul Shin,[†,∥] Dong Woo Lee,[†,∥] Kwang Yong Choi,[‡] Hyun-Joo Koo,[§] and Kang Min Ok*[,†]

[†]Department of Chemistry, Chung-Ang University, 221 Heukseok-dong, Dongjak-gu, Seoul 156-756, Republic of Korea

[‡]Department of Physics, Chung-Ang University, 221 Heukseok-dong, Dongjak-gu, Seoul 156-756, Republic of Korea

[§]Department of Chemistry and Research Institute for Basic Sciences, Kyung Hee University, Seoul 130-701, Republic of Korea

Supporting Information

ABSTRACT: A new vanadium antimony selenite, $VSb(SeO_3)_4$, has been synthesized through a solid-state reaction by using V_2O_5, Sb_2O_3, and SeO_2 as reagents. The crystal structure of $VSb(SeO_3)_4$ has been solved and refined by single-crystal X-ray diffraction. Whereas the starting V^{5+} cation has been reduced to V^{3+}, the Sb^{3+} cation has been oxidized to Sb^{5+} during the synthesis. $VSb(SeO_3)_4$ has a three-dimensional framework structure consisting of V/SbO_6 octahedra and SeO_3 groups. The V^{3+} and Sb^{5+} cations are statistically disordered in the same site with 50% occupancy. The oxide ligands in SeO_3 groups are shared by V/SbO_6 octahedra, and the framework expands outward radially from the center. The effective magnetic moment is estimated to be $\mu_{eff} = 2.57\ \mu_B$ per V^{3+} from the magnetic property measurements. The *g*-factor is determined to be $g = 1.9(4)$ from the electron paramagnetic resonance spectrum, which is typical for a d^2 ion. The spin-polarized DFT+U calculations with $U = 4$ and 5 eV exhibit the magnetic moments of 1.98 μ_B and 2.01 μ_B, respectively, on V^{3+} ion. Infrared and UV−vis diffuse reflectance spectra, elemental analysis, X-ray photoelectron spectroscopy, thermal analysis, and electronic structure calculations are also reported.

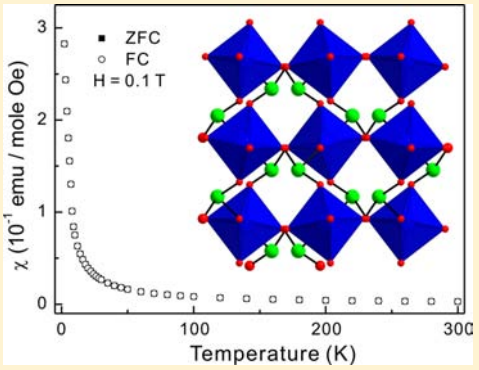

INTRODUCTION

Oxide materials containing a Se^{4+} cation, i.e., selenites, have attracted enormous attention attributable to their synthetic and structural versatilities. Thus, a great number of new mixed metal selenites have been synthesized thus far. In the syntheses of new selenites, the most commonly used starting material is selenium dioxide (SeO_2) that exhibits a lower triple point (340 °C) and very good solubility as an oxide.[1] When SeO_2 is combined with other metal oxides during the solid-state reactions, the accessible temperature and solubility allow it to be used as a flux for facile crystal growth.[2] Besides, SeO_2 reveals an excellent reactivity with other oxides, which enables it to be used in the formation of many novel materials. Meanwhile, the coordination of the Se^{4+} cation is also of particular interest. In extended oxide materials, the Se^{4+} cation normally shows a SeO_3 trigonal pyramidal coordination moiety. When the SeO_3 coordination geometry is amalgamated with other polyhedra such as tetrahedra or octahedra, the SeO_3 units often serve as linkers and generate a great deal of framework flexibilities.[3] Moreover, the Se^{4+} cation has asymmetric coordination geometry attributable to the stereoactive lone pair. In fact, the local asymmetric units are important building blocks for the formation of macroscopic noncentrosymmetric (NCS) materials. NCS materials are of topical interest attributed to their second-harmonic generation (SHG), ferroelectric, piezoelectric, and pyroelectric properties.[4] The incidence of crystallographic NCS in any new oxide material tends to be increased by combining two families of second-order Jahn−Teller distortive cations,[5] i.e., lone pair cations (Sb^{3+}, Se^{4+}, Te^{4+}, I^{5+}, etc.) and octahedrally coordinated d^0 transition metal cations (Ti^{4+}, V^{5+}, Nb^{5+}, Mo^{6+}, etc.). However, a material with an extended structure may crystallize in macroscopic centrosymmetric (CS) structure when the local asymmetric groups align in an antiparallel manner. Recently, several factors deciding the space group centricities have been reported, where the framework flexibility, the hydrogen-bonds, and the size of metal cations are crucial.[3h,6] Further investigations in order to design functional materials rationally by controlling the overall centricities, however, remain ongoing challenges. We have chosen to investigate the V^{5+}−Sb^{3+}−Se^{4+}−oxide system by combining V_2O_5, Sb_2O_3, and SeO_2 as starting reagents. During the exploratory synthesis reactions, we discovered a highly symmetric three-dimensional selenite, $VSb(SeO_3)_4$, in which the V^{5+} reduced to V^{3+} and the Sb^{3+} oxidized to Sb^{5+}. Although many vanadium selenites have been reported, $VSb(SeO_3)_4$ is the first example of a selenite material containing V^{3+} cations. In this Article, we report phase pure synthesis, structure determination, elemental analysis, infrared and UV−vis diffuse reflectance spectra, X-ray photoelectron spectroscopy, thermal analysis, and dipole moment calculations of $VSb(SeO_3)_4$. Since the reported material contains a d^2 cation (V^{3+}), dc

Received: August 22, 2013
Published: November 21, 2013

   dx.doi.org/10.1021/ic4021564 | *Inorg. Chem.* 2013, 52, 14224−14230

magnetization and electron paramagnetic resonance (EPR) measurements are also reported as are electronic structure calculations.

EXPERIMENTAL SECTION

Reagents. V_2O_5 (Junsei, 99.0%), SeO_2 (Aldrich, 99.8%), and Sb_2O_3 (Aldrich, 99%) were used as received.

Synthesis. Crystals of $VSb(SeO_3)_4$ were prepared using a standard solid-state reaction method. A 0.046 g (2.50×10^{-4} mol) portion of V_2O_5, 0.073 g (2.50×10^{-4} mol) of Sb_2O_3, and 0.333 g (3.00×10^{-3} mol) of SeO_2 were mixed thoroughly with an agate mortar and pestle. The reaction mixture was then transferred into a silica tube that was evacuated and sealed. The tube was slowly heated to 380 °C for 5 h, 600 °C for 48 h, and cooled to 400 °C at a rate of 6 °C h^{-1} before being quenched to room temperature. The products contained green octahedral-shaped crystals of $VSb(SeO_3)_4$ with polycrystalline $SbVO_4$ and some amorphous phases. A pure polycrystalline sample of $VSb(SeO_3)_4$ was synthesized through the same solid-state reaction with stoichiometric amounts of reactants in a sealed fused silica tube. The stoichiometric reaction mixture in the sealed tube was heated to 400 °C for 36 h with two intermediate regrindings. Powder X-ray diffraction data on the final polycrystalline sample are in good agreement with the calculated pattern from the single-crystal analysis (see the Supporting Information).

Single Crystal X-ray Diffraction. A standard crystallographic method was used to determine the crystal structure of $VSb(SeO_3)_4$ with a green trigonal plate ($0.012 \times 0.023 \times 0.032$ mm^3). The data were obtained at room temperature using a Bruker SMART BREEZE diffractometer that is equipped with a 1K CCD area detector using graphite monochromated Mo Kα radiation. A hemisphere of data was collected using a narrow-frame method with an exposure time of 5 s/frame and scan widths of 0.30° in ω. In order to monitor instrument and crystal stability, the first 50 frames were remeasured at the end of the data collection. The maximum correction applied to the intensities was <1%. The SAINT program was used to integrate the data,[7] and the intensities were corrected for air absorption, polarization, Lorentz factor, and absorption due to the variation in the path length through the detector faceplate. A semiempirical absorption correction was applied on the hemisphere of data using the SADABS program.[8] The data were solved using SHELXS-97[9] and refined with SHELXL-97.[10] All atoms were refined with anisotropic displacement parameters and converged for $I > 2\sigma(I)$. The WinGX-98 crystallographic software package was used for all calculations.[11] Detailed crystallographic information and selected bond distances and angles for $VSb(SeO_3)_4$ are given in Tables 1–3.

Powder X-ray Diffraction. The phase purity of the synthesized material was confirmed by powder X-ray diffraction. The XRD pattern was obtained on a Bruker D8-Advance diffractometer using Cu Kα radiation with 40 kV and 40 mA at room temperature. The powder sample was loaded on a sample holder and scanned in the 2θ range 5–70° with a step time of 0.2 s, and a step size of 0.02°.

Table 1. Crystallographic Data for $VSb(SeO_3)_4$

formula	$V_{0.5}Sb_{0.5}Se_2O_6$
fw	340.26
space group	$Pa\bar{3}$ (No. 205)
$a = b = c$ (Å)	8.0301(7)
V (Å^3)	517.80(8)
Z	4
T (K)	298.0(2)
λ (Å)	0.710 73
ρ_{calcd} (g cm^{-3})	4.365
μ (mm^{-1})	17.632
$R(F)^a$	0.0285
$R_w(F_o^2)^b$	0.0401

$^aR(F) = \Sigma||F_o| - |F_c||/\Sigma|F_o|$. $^bR_w(F_o^2) = [\Sigma w(F_o^2 - F_c^2)^2/\Sigma w(F_o^2)^2]^{1/2}$.

Scanning Electron Microscope/Energy Dispersive Analysis by X-ray (SEM/EDAX). A Hitachi S-3400N/Horiba Energy EX-250 instrument has been used for SEM/EDAX. EDAX for $VSb(SeO_3)_4$ reveals a V/Sb/Se ratio of 1.0:1.1:4.0.

Infrared Spectroscopy. Infrared spectral data were acquired on a Varian 1000 FT-IR spectrometer in the 400–4000 cm^{-1} range, with the sample embedded in a KBr matrix.

UV–Vis Diffuse Reflectance Spectroscopy. UV–vis reflectance data were collected on a Hyperion 3000 FT-UV–vis–IR microscope attached to a Bruker Vertex 80 spectrometer over the spectral range 330–1100 nm at room temperature at the Korea Basic Science Institute. The Kubelka–Munk function was used to convert the reflectance spectrum to the absorbance.[12]

X-ray Photoelectron Spectroscopy (XPS). XPS spectra were collected using a Thermo VG K-alpha spectrometer at a base pressure better than 2.9×10^{-9} mbar at room temperature with Al Kα monochromated X-rays having energy of 1486.6 eV. The instrument resolution was 0.78 eV, and the X-ray power was 12 kV and 3 mA.

Thermogravimetric Analysis. Thermal properties of the reported material were analyzed by a Setaram LABSYS TG-DTA/DSC thermogravimetric analyzer. The polycrystalline $VSb(SeO_3)_4$ sample was loaded in an alumina crucible and heated at a rate of 10 °C min^{-1} from room temperature to 800 °C under flowing argon.

Magnetic Measurements. The magnetic susceptibilities of the polycrystalline $VSb(SeO_3)_4$ were measured by using a Quantum Design Magnetic Property Measurement System (MPMS) SQUID magnetometer in the temperature range 2–300 K, and the magnetization curve (M versus H) was measured at 2 K by sweeping an external magnetic field from 0 to 7 T.

Electron Paramagnetic Resonance (EPR) Measurements. EPR experiments were performed at an X-band by using JEOL JES-FA200 spectrometer at room temperature.

Theoretical Calculations. The electronic structure of $VSb(SeO_3)_4$ was studied on the basis of spin-polarized density functional theory (DFT) calculations. The projected augmented wave method encoded in the Vienna ab initio simulation package,[13] Burke and Ernzerhof[14] for the exchange-correlation correction with the plane wave cutoff energy of 450 eV, the generalized gradient approximation (GGA) of Perdew, the threshold 10^{-6} eV for self-consistent-field energy convergence, and a set of $8 \times 8 \times 8$ k points were employed. The DFT plus on-site repulsion U (DFT+U) method[15] was applied to describe the electron correlation associated with V 3d states with $U = 4$ and 5 eV. For optimization of the crystal structure of $VSb(SeO_3)_4$, only the atom positions were optimized on the basis of DFT+U calculation with force convergence threshold of 0.05 eV/Å.

RESULTS AND DISCUSSION

Synthesis. The reaction of V_2O_5, Sb_2O_3, and SeO_2 in vacuum at 400 °C results in the formation of $V^{3+}Sb^{5+}(SeO_3)_4$. While the starting V^{5+} cation has been reduced to V^{3+}, Sb^{3+} cation has been oxidized to Sb^{5+} during the solid-state reaction. As we will discuss in more detail later, the formation of V^{3+} through the redox reaction can be confirmed by magnetic susceptibility measurements, EPR measurements, XPS, and theoretical calculations. In fact, similar redox processes have been observed before from the synthesis reactions for antimony vanadates materials.[16] We were also able to synthesize $VSb(SeO_3)_4$ directly through a solid-state reaction using a stoichiometric amount of V_2O_3, Sb_2O_5, and SeO_2 in a sealed fused silica tube, which unequivocally confirms the cations' oxidation states in the reported material.

Structure. $VSb(SeO_3)_4$ is a novel mixed metal selenite material crystallizing in a cubic space group, $Pa\bar{3}$ (No. 205). The material exhibits a three-dimensional framework that consists of V/SbO_6 octahedra and SeO_3 polyhedra (see Figure 1). The V^{3+} and Sb^{5+} cations are statistically disordered in the same site (4b) with 50% occupancy. The unique V^{3+} or Sb^{5+}

dx.doi.org/10.1021/ic4021564 | Inorg. Chem. 2013, 52, 14224–14230

Table 2. Atomic Coordinates and Equivalent Isotropic Displacement Parameters (Å^2) for $VSb(SeO_3)_4$

	x	y	z	U_{eq}[a]	occupancy
Se(1)	0.167 34(8)	0.167 34(8)	0.167 34(8)	0.0167(3)	1.0
V(1)/Sb(1)	0.5	0	0	0.0127(4)	0.5/0.5
O(1)	0.2582(5)	0.0318(5)	0.0317(5)	0.0212(11)	1.0

[a] U_{eq} is defined as one-third of the trace of the orthogonalized U_{ij} tensor.

Table 3. Bond Lengths (Å) and Angles (deg) for $VSb(SeO_3)_4$

Se(1)−O(1) × 3	1.704(4)	O(1)−Se(1)−O(1) × 3	97.98(19)
Sb(1)−O(1) × 3	1.975(4)	O(1)−Sb(1)−O(1) × 6	89.06(18)
		O(1)−Sb(1)−O(1) × 6	90.94(18)
		O(1)−Sb(1)−O(1)	180.00(5)
		O(1)−Sb(1)−O(1)	180.0(2)
		O(1)−Sb(1)−O(1)	180.0(3)

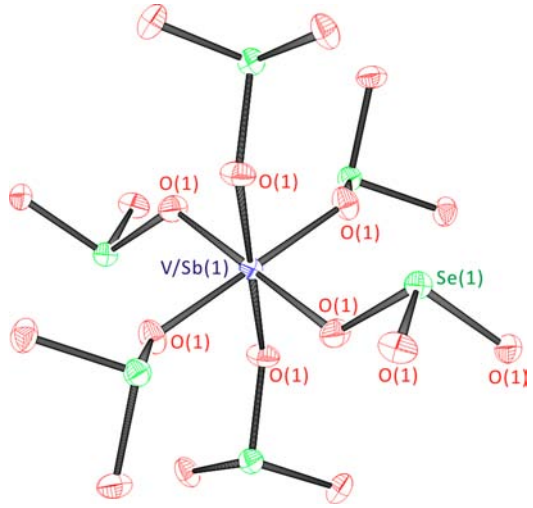

Figure 1. ORTEP (50% probability ellipsoids) drawing for V/SbO_6 octahedra and SeO_3 polyhedra in $VSb(SeO_3)_4$.

cation is connected to six oxygen atoms in octahedral coordination environment with V^{3+}/Sb^{5+}−O bond lengths of 1.975(4) Å. The observed O− (V^{3+}/Sb^{5+})−O bond angles range from 89.06(18)° to 180.0(3)°. The unique Se^{4+} cation is linked to three oxygen atoms and reveals three-coordinate SeO_3 polyhedra. The SeO_3 polyhedra exhibit asymmetric coordination moiety owing to the stereoactive lone pairs. The observed Se^{4+}−O bond distances are 1.704(4) Å, and the O−Se^{4+}−O bond angles are 97.98(19)°.

As can be seen in Figure 2a, the V^{3+} or Sb^{5+} cation is in the center of the oxide octahedron. Then, all of the corners of the octahedron are shared by Se^{4+} cations with trigonal pyramidal coordination environment (Figure 2b). The oxide ligands in SeO_3 groups are further shared by V/SbO_6 octahedra, and the framework expands outward radially from the center (Figure 2c,d). Interestingly, the lone pairs on SeO_3 groups located *trans* to each other are pointed in opposite directions, which results in cancellation of the local dipole moments, rendering the material centrosymmetric (Figure 2e). In connectivity terms, the structure of $VSb(SeO_3)_4$ may be formulated as a neutral framework of $\{0.5[V^{3+}O_{6/2}]^{3-}0.5[Sb^{5+}O_{6/2}]^{-}2[Se^{4+}O_{3/2}]^{+}\}^0$. Bond valence sum calculations[17] resulted in values of 3.09, 4.99, 4.02, and 2.01 for V^{3+}, Sb^{5+}, Se^{4+}, and O^{2-}, respectively.

It is worth comparing the structure of $VSb(SeO_3)_4$ with known V^{4+}-selenites such as $VOSe_2O_5$ and $VO(SeO_2OH)_2$.[18] All three materials exhibit three-dimensional framework structures consisting of VO_6 octahedra and selenite linkers. However, the coordination environment around vanadium cations are completely different: while $VSb(SeO_3)_4$ contains discrete $V^{3+}O_6$ moieties in perfect octahedral coordination environments, $VOSe_2O_5$ and $VO(SeO_2OH)_2$ reveal chains of corner-shared VO_6 octahedra with C_4-type octahedral distortions.

Thermogravimetric Analysis. The thermal property of $VSb(SeO_3)_4$ was monitored using thermogravimetric analysis. TGA measurement on a polycrystalline sample of $VSb(SeO_3)_4$ shows that the material is stable up to 370 °C. After the temperature, $VSb(SeO_3)_4$ starts decomposing, attributable to the loss of SeO_2, calculated (experimental): 65.4% (65.2%). An endothermic peak in the heating curve of the differential thermal analysis curve confirms the sublimation of SeO_2. The powder XRD measurement confirmed that the decomposed material was $SbVO_4$.[19] The TGA curve for the reported material has been deposited in the Supporting Information.

Infrared (IR) Spectroscopy. The IR spectrum of $VSb(SeO_3)_4$ revealed V−O vibrations in the region of *ca.* 700 and 875 cm^{-1}. In addition, Se−O vibrations were observed at about 466 and 557 cm^{-1}. The strong band occurring at 764 cm^{-1} is attributable to the Sb−O and/or V−O vibrations. The assignments are well matched with those previously reported.[20] The IR spectrum for the reported material has been deposited as Supporting Information.

UV−Vis Diffuse Reflectance Spectroscopy. UV−vis diffuse reflectance spectral data were collected on $VSb(SeO_3)_4$ (see the Supporting Information). The following Kubelka−Munk function was used to calculate absorption (K/S) data[12]

$$F(R) = \frac{(1-R)^2}{2R} = \frac{K}{S}$$

in which S is the scattering, K the absorption, and R the reflectance. In the (K/S)-versus-E plot, extrapolating the linear region of the rising curve to zero suggested the onset of absorption at approximately 2.4 eV, which is the optical band gap energy for $VSb(SeO_3)_4$. The overall band gap for the reported material may be due to the degree of V (3d) and Sb (5s) orbitals that are engaged in the conduction bands. A couple of broad peaks in the region 1.1−2.2 eV are attributed to d−d transitions of the V^{3+} cations.

X-ray Photoelectron Spectroscopy (XPS). XPS spectra have been obtained to confirm the valence states of the constituent elements. The broad peak at 516.5 eV corresponds to the binding energy (BE) of V^{3+} $2p_{3/2}$, while the peaks at 531.4 and 540.9 eV exhibit the BE of Sb^{5+} $3d_{5/2}$ and $3d_{3/2}$, respectively. A band occurring at 59.5 eV is attributed to the BE of Se^{4+} $3d_{5/2}$. The assignments are consistent with those reported values.[21] The XPS spectra for the reported material have been deposited in the Supporting Information.

Direct Current Magnetization Measurements. The temperature dependence of the magnetic susceptibility, $\chi(T)$, was measured in the range 2−300 K under an external field of H = 0.1 T (see Figure 3). With decreasing temperature, the

dx.doi.org/10.1021/ic4021564 | *Inorg. Chem.* 2013, 52, 14224−14230

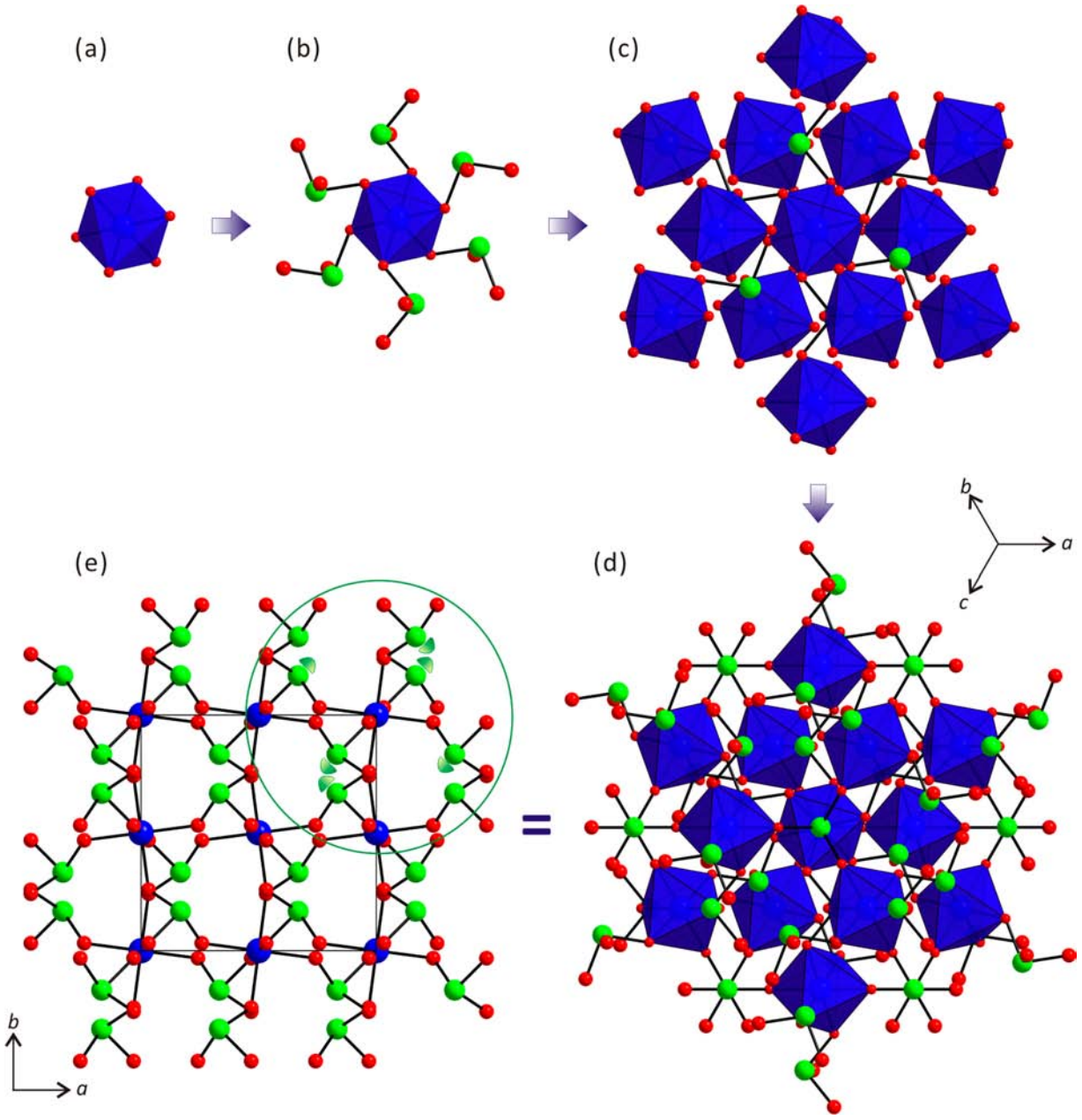

Figure 2. Ball-and-stick and polyhedral representations of $VSb(SeO_3)_4$ (blue, V/Sb; green, Se; red, O). Note that all of the corners of V/SbO_6 octahedron (a) are shared by SeO_3 groups (b). Further, the corners of SeO_3 groups are shared by Sb/VO_6 octahedra, and the framework expands outward radially (c and d). The lone pairs on SeO_3 groups located *trans* to each other are oriented in opposite directions (e).

susceptibility steeply increases like a paramagnet. We find no difference between ZFC and FC measurements and no magnetic transition down to T = 2 K. As seen from the inverse susceptibility in the inset of Figure 3a, $\chi(T)$ is well-described by the Curie–Weiss law, $\chi(T) = C/(T - \theta_{CW}) + \chi_0$ where C, θ_{CW}, and χ_0 are the Curie constant, the Curie–Weiss temperature, and the temperature-independent term occurring from the diamagnetism of the core electron shells and the van Vleck paramagnetism of the open shells of the V^{3+} ions, respectively. A fit to the Curie–Weiss law yields C = 0.82(4) emu mol^{-1}, $\theta_{CW} = -1.10(4)$ K, and $\chi_0 = 2.02(2) \times 10^{-4}$ emu mol^{-1} Oe^{-1}. The effective magnetic moment is estimated to be $\mu_{eff} = 2.57\ \mu_B$, which is very close to the spin-only value of $\mu_{theor} = 2.76\ \mu_B$ per V^{3+}. The tiny negative value of θ_{CW} indicates a weak antiferromagnetic coupling between the V^{3+} ions. The smallness of θ_{CW} is due to the site disorders between the V^{3+} and Sb^{5+} ions. In this case, the exchange constant is given by a supersuperexchange (SSE) interaction of the V^{3+} ions. Because in a mean-field theory a magnetic transition temperature is given by θ_{CW}, the antiferromagnetic ordering is expected to occur for temperatures below 1 K, if present.

Isothermal magnetization curve $M(H)$ was measured at 2 K (see Figure 3b). In the paramagnetic state the magnetization increases rather steeply with increasing field up to 3.5 T and then increases slowly. We observe no hysteresis behavior between the up and the down sweep. At H = 7 T, the magnetization does not reach a saturated magnetic moment of $M_s = gS\mu_B = 1.94\ \mu_B$. At this temperature the magnetization curve is not described by a Brillouin function possibly due to a development of short-range magnetic correlations. Indeed,

dx.doi.org/10.1021/ic4021564 | *Inorg. Chem.* 2013, 52, 14224–14230

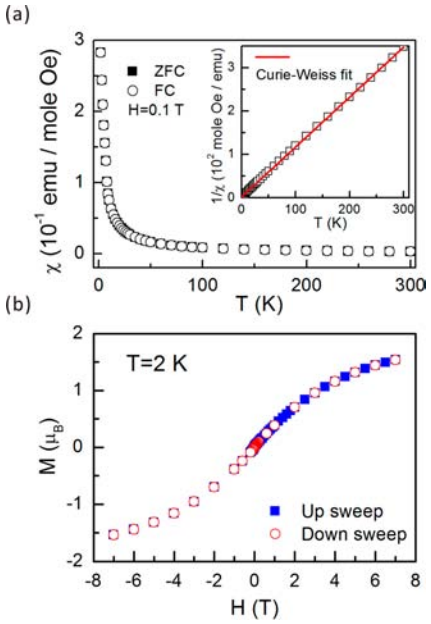

Figure 3. (a) Magnetic susceptibilities measured in an external field of H = 0.1 T in the temperature range T = 2−300 K. Inset shows temperature dependence of the inverse magnetic susceptibility with a Curie−Weiss fit (red line). (b) The magnetization hysteresis curve (M versus H) measured at 2 K and in external magnetic fields from −7 to +7 T.

$\chi(T)$ deviates from the Curie−Weiss law at the respective temperature.

EPR Measurements. Figure 4 shows the EPR spectrum of the polycrystalline $VSb(SeO_3)_4$ measured at an X-band

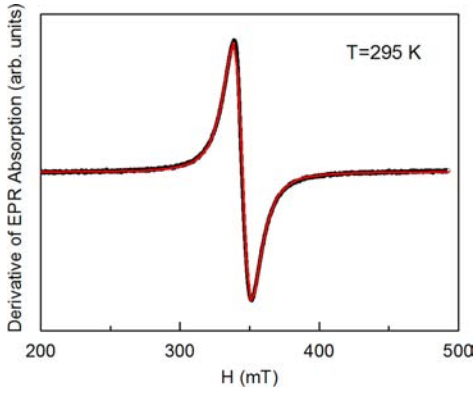

Figure 4. Derivative of the EPR absorption of the polycrystalline $VSb(SeO_3)_4$ measured at an X-band frequency and T = 295 K. The solid red line is a fit to a single Lorentzian profile.

frequency and at T = 295 K. We find that the EPR spectrum is well-fitted by a single Lorentzian profile (see the solid line) rather than a multiple Lorentzian one. The g-factor is determined to be g = 1.9(4), which is typical for d^2 ions.[22] The single resonance line is rather unusual for the polycrystalline sample and indicates that anisotropies of the V^{3+} ions are extremely small due to the powder average of V^{3+} local environments and the statistical disorders of the V^{3+} and Sb^{5+} cations. In addition, a Lorentzian line-shape means that the EPR signal is exchange-narrowed due to fast electronic fluctuations of V^{3+} ions induced by an exchange interaction. Therefore, the statistical disorders of the V^{3+} and Sb^{5+} cations should be discriminated from a random distribution of the V^{3+} cations, leading to a Gaussian profile rather than a Lorentzian one.

Electronic Structure Calculations. The projected density of states (PDOS) plots calculated for the optimized structure of $VSb(SeO_3)_4$ is presented in Figure 5. The PDOS plot shows

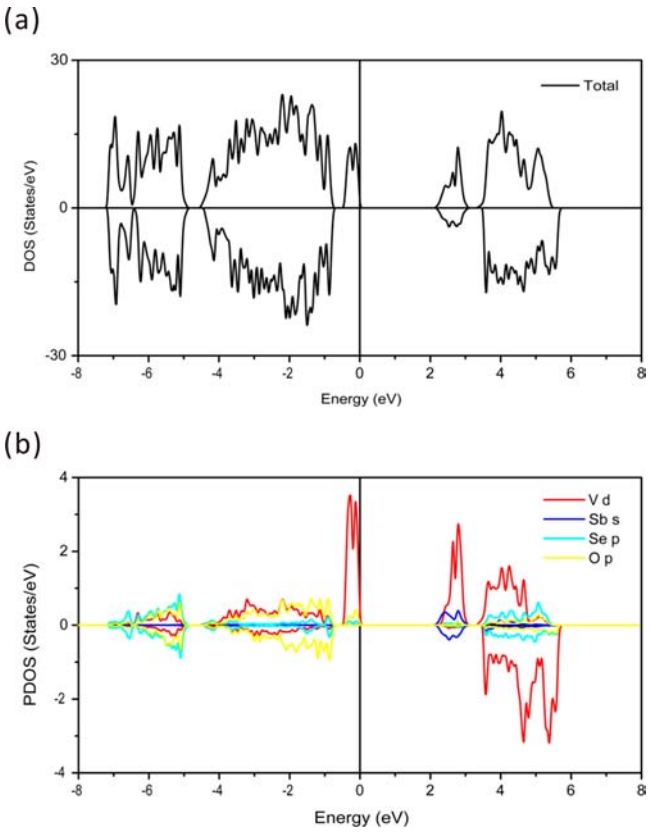

Figure 5. Plots of (a) total density of states and (b) partial density of states obtained for the optimized structure of $VSb(SeO_3)_4$ from DFT +U calculation with U = 4 eV.

that the up spin states of V 3d are in both regions of below and above the Fermi level, while the down spin states of V 3d are above the Fermi level. This fact indicates that 3d states of V are partly filled and the vanadium atom is not pentavalent ion, V^{5+}. Also, broad peaks observed in the region 1.1−2.2 eV from the diffuse reflectance spectrum may be attributable to transitions between up spin states of V 3d to the down spin states of V3d. In addition, we obtained the magnetic moments of 1.98 μ_B and 2.01 μ_B on V ion from the spin-polarized DFT+U calculation with U = 4 and 5 eV, respectively. From these findings, we can expect that the V atoms in $VSb(SeO_3)_4$ are V^{3+} ions containing S = 1 spin.

Magnetic Structure Determination. For spin exchange interaction of $VSb(SeO_3)_4$, we consider only the nearest spin exchange path J made up of $(VO_6)-(SeO_3)-(VO_6)$ super-superexchange path since the (VO_6) octahedral units are isolated and they are connected by SeO_3 units in $VSb(SeO_3)_4$ layer. To obtain the value of the spin exchange parameter J, the relative energies of the two ordered spin states FM and AF in Figure 6 is determined on the basis of DFT+U calculations with U = 4 and 5 eV. The relative energies of the spin states calculated from DFT+U calculation are listed in Table 4. In

dx.doi.org/10.1021/ic4021564 | Inorg. Chem. 2013, 52, 14224−14230

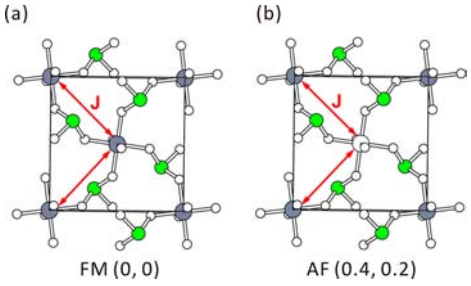

Figure 6. Ordered spin arrangements of (a) FM and (b) AF states, where the gray and large white circles represent the up spin and down spin sites of V^{3+} ion, respectively. The red arrows indicate the spin exchange path *J*.

Table 4. Relative Energies (in meV/formula unit), Spin Exchange Parameter *J* (in K), and Curie–Weiss Temperature (in K) Obtained for the Optimized Structure of $VSb(SeO_3)_4$ from DFT+U Calculations

U (eV)	4	5
FM	0	0
AF	0.4	0.2
J/k_B	1.2	0.6
θ	3.2	1.6

terms of the spin Hamiltonian, the total spin-exchange energies of these states are represented as

$$E_{FM} = -4J(N^2/4)$$

$$E_{AF} = 4J(N^2/4)$$

by using energy expressions obtained for spin dimers with *N* unpaired spins per spin site (in the present case, $N = 2$).[23] Thus, we obtained the values of *J* summarized in Table 4 by mapping the relative energies of the two ordered spin states onto the corresponding energies expected from the total spin exchange energies.[24] *J* is very weak and ferromagnetic for all *U* values employed. In the mean field theory, which is valid in the paramagnetic limit, the Curie–Weiss temperature θ is related to the spin exchange parameter of $VSb(SeO_3)_4$ as follows:

$$\theta_{cal} = \frac{S(S+1)}{3k_B}\sum_i z_i J_i = \frac{2}{3k_B}(4J)$$

The Curie–Weiss temperatures θ_{cal} estimated with the calculated spin exchange parameter are 3.2 and 1.6 K from the DFT+U calculations with $U = 4$ and 5 eV, respectively (see Table 4). They are small positive values which indicate that a weak ferromagnetic interaction is dominant in $VSb(SeO_3)_4$. It is consistent with the experiment that the calculated θ_{cal} values are very small. However, the sign of the Curie–Weiss temperature is inconsistent with the experimental observation. For a given magnetic solid, spin exchange interactions strongly depend on its crystal structure. Therefore, the magnitude as well as the sign of the *J* can vary sensitively with change of a crystal structure. In addition, if the next-next-nearest spin exchange paths J_{NNN} through $(VO_6)-(SeO_3)-(SbO_6)-(SeO_3)-(VO_6)$ ($8J_{NNN}$) are weakly AFM and $|J_{NNN}| > (1/2)|J|$ we can expect small negative value of the θ_{cal}. Although the spin–orbital coupling could be strong for the V^{3+} cation; however, it may be diminished by statically disordered Sb^{5+} cations. Thus, it would be very difficult to determine whether the exchange coupling is ferromagnetic or antiferromagnetic in the present case.

Dipole Moment Calculations. $VSb(SeO_3)_4$ possesses cations in asymmetric coordination environment, Se^{4+}, in the framework. Although the material crystallizes in a centrosymmetric space group, it would be worth investigating the magnitude and direction of the distortions in the polyhedra of lone pair cation to fully understand their local asymmetric moiety. Thus, the local dipole moment for Se^{4+} in $VSb(SeO_3)_4$ has been calculated by using the method described earlier with bond valence sum approach.[25] We found that the local dipole moment for the unique $Se(1)O_3$ polyhedron is calculated to be approximately 9.3 D (D = Debyes), which is consistent with those reported values for SeO_3 polyhedra.[26]

CONCLUSIONS

A new vanadium(III) antimony(V) selenium(IV) oxide material, $VSb(SeO_3)_4$, has been successfully synthesized by a standard solid-state reaction. A redox reaction occurred during the synthesis such that the V^{5+} reduced to V^{3+} and the Sb^{3+} oxidized to Sb^{5+}. Crystallographic data indicate that $VSb(SeO_3)_4$ exhibits a three-dimensional framework with V/SbO_6 octahedra and SeO_3 polyhedra. The temperature dependence magnetization measurements indicate $VSb(SeO_3)_4$ has a weak antiferromagnetic coupling between the V^{3+} ions. An exchange-narrowed Lorentzian line shape is observed from the EPR, which is attributable to fast electronic fluctuations of V^{3+} ions induced by an exchange interaction. Electronic structure calculations shows that 3d states of V are partly filled, which confirms the vanadium ion is not V^{5+} but V^{3+}. The relative energies of the two ordered spin states FM and AF were determined by DFT+U calculations, and the extracted values of the spin exchange parameter *J* turn out to be weak attributed to the statistical disorders of the V^{3+} and Sb^{5+} cations.

ASSOCIATED CONTENT

Supporting Information

X-ray crystallographic file in CIF format, calculated and observed X-ray diffraction patterns, thermogravimetric analysis diagram, IR spectrum, and UV–vis diffuse reflectance spectrum for $VSb(SeO_3)_4$. This material is available free of charge via the Internet at http://pubs.acs.org.

AUTHOR INFORMATION

Corresponding Author

*E-mail: kmok@cau.ac.kr. Phone: +82-2-820-5197. Fax: +82-2-825-4736.

Author Contributions

‖These two authors contributed equally to this work and are co-first-authors.

Notes

The authors declare no competing financial interest.

ACKNOWLEDGMENTS

This research was supported by Basic Science Research Program through the National Research Foundation of Korea (NRF) funded by Ministry of Education, Science & Technology (Grants 2013R1A2A2A01007170, 2009-0093817, 2012-046138, and 2010-0021042).

REFERENCES

(1) *CRC Handbook of Chemistry and Physics, Internet Version 2005*; Lide, D. R., Ed.; CRC Press: Boca Raton, FL, 2005.

(2) (a) Ok, K. M.; Halasyamani, P. S. *Chem. Mater.* **2002**, *14*, 2360−2364. (b) Shen, Y. L.; Jiang, H. L.; Xu, J.; Mao, J.-G.; Cheah, K. W. *Inorg. Chem.* **2005**, *44*, 9314−9321. (c) Zhang, W.; Tao, X.; Zhang, C.; Gao, Z.; Zhang, Y.; Yu, W.; Cheng, X.; Liu, X.; Jiang, M. *Cryst. Growth Des.* **2008**, *8*, 304−307.

(3) (a) Harrison, W. T. A.; Dussack, L. L.; Jacobson, A. J. *Inorg. Chem.* **1994**, *33*, 6043−6049. (b) Vaughey, J. T.; Harrison, W. T. A.; Dussack, L. L.; Jacobson, A. J. *Inorg. Chem.* **1994**, *33*, 4370−4375. (c) Porter, Y.; Halasyamani, P. S. *J. Solid State Chem.* **2003**, *174*, 441−449. (d) Sivakumar, T.; Chang, H. Y.; Baek, J.; Halasyamani, P. S. *Chem. Mater.* **2007**, *19*, 4710−4715. (e) Jiang, H.; Kong, F.; Fan, Y.; Mao, J.-G. *Inorg. Chem.* **2008**, *47*, 7430−7437. (f) Chang, H. Y.; Kim, S. W.; Halasyamani, P. S. *Chem. Mater.* **2010**, *22*, 3241−3250. (g) Li, P.-X.; Zhang, S.-Y.; Mao, J.-G. *Dalton Trans.* **2010**, *39*, 11560−11567. (h) Oh, S.-J.; Lee, D. W.; Ok, K. M. *Inorg. Chem.* **2012**, *51*, 5393−5399. (i) Oh, S.-J.; Lee, D. W.; Ok, K. M. *Dalton Trans.* **2012**, *41*, 2995−3000.

(4) (a) Jona, F.; Shirane, G. *Ferroelectric Crystals*; Pergamon Press: Oxford, U.K., 1962. (b) Cady, W. G. *Piezoelectricity; An Introduction to the Theory and Applications of Electromechanical Phenomena in Crystals*; Dover: New York, 1964. (c) Lang, S. B. *Sourcebook of Pyroelectricity*; Gordon & Breach Science: London, 1974; (d) Ok, K. M.; Chi, E. O.; Halasyamani, P. S. *Chem. Soc. Rev.* **2006**, *35*, 710−717.

(5) (a) Opik, U.; Pryce, M. H. L. *Proc. R. Soc. London* **1957**, *A238*, 425−447. (b) Bader, R. F. W. *Mol. Phys.* **1960**, *3*, 137−151. (c) Pearson, R. G. *THEOCHEM* **1983**, *103*, 25−34. (d) Wheeler, R. A.; Whangbo, M.-H.; Hughbanks, T.; Hoffmann, R.; Burdett, J. K.; Albright, T. A. *J. Am. Chem. Soc.* **1986**, *108*, 2222−2236.

(6) (a) Sykora, R. E.; Ok, K. M.; Halasyamani, P. S.; Albrecht-Schmitt, T. E. *J. Am. Chem. Soc.* **2002**, *124*, 1951−1957. (b) Goodey, J.; Ok, K. M.; Broussard, J.; Hofmann, C.; Escobedo, F. V.; Halasyamani, P. S. *J. Solid State Chem.* **2003**, *175*, 3−12. (c) Ok, K. M.; Baek, J.; Halasyamani, P. S.; O'Hare, D. *Inorg. Chem.* **2006**, *45*, 10207−10214. (d) Choi, M.-H.; Kim, S.-H.; Chang, H. Y.; Halasyamani, P. S.; Ok, K. M. *Inorg. Chem.* **2009**, *48*, 8376−8382. (e) Lee, D. W.; Bak, D.-b.; Kim, S. B.; Kim, J.; Ok, K. M. *Inorg. Chem.* **2012**, *51*, 7844−7850. (f) Lee, D. W.; Ok, K. M. *Inorg. Chem.* **2013**, *52*, 5176−5184.

(7) *SAINT, Program for Area Detector Absorption Correction, Version 4.05*; Siemens Analytical X-ray Instruments: Madison, WI, 1995.

(8) Blessing, R. H. *Acta Crystallogr.* **1995**, *A51*, 33−38.

(9) Sheldrick, G. M. *SHELXS-97—A Program for Automatic Solution of Crystal Structures*; University of Göttingen: Göttingen, Germany, 1997.

(10) Sheldrick, G. M. *SHELXL-97—A Program for Crystal Structure Refinement*; University of Göttingen: Göttingen, Germany, 1997.

(11) Farrugia, L. J. *J. Appl. Crystallogr.* **1999**, *32*, 837−838.

(12) (a) Kubelka, P.; Munk, F. *Z. Tech. Phys.* **1931**, *12*, 593−601. (b) Tauc, J. *Mater. Res. Bull.* **1970**, *5*, 721−730.

(13) (a) Kresse, G.; Hafner, J. *Phys. Rev. B* **1993**, *47*, 558−561. (b) Kresse, G.; Furthmüller, J. *Comput. Mater. Sci.* **1996**, *6*, 15−50. (c) Kresse, G.; Furthmüller, J. *Phys. Rev. B* **1996**, *54*, 11169−11186.

(14) Perdew, J. P.; Burke, K.; Ernzerhof, M. *Phys. Rev. Lett.* **1996**, *77*, 3865−3868.

(15) Dudares, S. L.; Botton, G. A.; Savrasov, S. Y.; Humphreys, C. J.; Sutton, A. P. *Phys. Rev. B* **1998**, *57*, 1505−1509.

(16) (a) Hansen, S.; Stahl, K.; Nilsson, R.; Andersson, A. *J. Solid State Chem.* **1993**, *102*, 340−348. (b) Landa-Canovas, A.; Nilsson, J.; Hansen, S.; Stahl, K.; Andersson, A. *J. Solid State Chem.* **1995**, *116*, 369−377.

(17) (a) Kim, S.-H.; Halasyamani, P. S.; Melot, B. C.; Seshadri, R.; Green, M. A.; Sefat, A. S.; Mandrus, D. *Chem. Mater.* **2010**, *22*, 5074−5083. (b) Kim, S.-H.; Yeon, J.; Sefat, A. S.; Mandrus, D. G.; Halasyamani, P. S. *Chem. Mater.* **2010**, *22*, 6665−6672.

(18) (a) Brown, I. D.; Altermatt, D. *Acta Crystallogr.* **1985**, *B41*, 244−247. (b) Brese, N. E.; O'Keeffe, M. *Acta Crystallogr.* **1991**, *B47*, 192−197.

(19) Landa-Canovas, A. R.; Hansen, S.; Stahl, K. *Acta Crystallogr.* **1997**, *B53*, 221−230.

(20) (a) Xiong, H.-M.; Chen, J.-S.; Li, D.-M. *J. Mater. Chem.* **2003**, *13*, 1994−1998. (b) Ok, K. M.; Halasyamani, P. S. *Inorg. Chem.* **2005**, *44*, 2263−2271. (c) Lee, D. W.; Oh, S.-J.; Halasyamani, P. S.; Ok, K. M. *Inorg. Chem.* **2011**, *50*, 4473−4480.

(21) (a) Malmsten, G.; Thoren, I.; Hogberg, S.; Bergmark, J. E.; Karlsson, S. E. *Phys. Scr.* **1971**, *3*, 96−100. (b) Morgan, W. E.; Stec, W. J.; van Wazer, J. R. *Inorg. Chem.* **1973**, *12*, 953−955. (c) Horvath, B.; Strutz, J.; Geyer-Lippmann, J.; Horvath, E. G. *Z. Anorg. Allg. Chem.* **1981**, *483*, 181−192.

(22) Abragam, A.; Bleaney, B. *Electron Paramagnetic Resonance of Transition*, reprint ed.; Oxford University Press: Oxford, U.K., 2012.

(23) (a) Dai, D.; Whangbo, M.-H. *J. Chem. Phys.* **2001**, *114*, 2887−2893. (b) Dai, D.; Whangbo, M.-H. *J. Chem. Phys.* **2003**, *118*, 29−39.

(24) Whangbo, M.-H.; Koo, H.-J.; Dai, D. *J. Solid State Chem.* **2003**, *176*, 417−481.

(25) (a) Meunier, G.; Galy, J. *Acta Crystallogr.* **1971**, *B27*, 602−607. (b) Maggard, P. A.; Nault, T. S.; Stern, C. L.; Poeppelmeier, K. R. *J. Solid State Chem.* **2003**, *175*, 27−33. (c) Izumi, H. K.; Kirsch, J. E.; Stern, C. L.; Poeppelmeier, K. R. *Inorg. Chem.* **2005**, *44*, 884−895.

(26) (a) Lee, D. W.; Kim, S. B.; Ok, K. M. *Inorg. Chem.* **2012**, *51*, 8530−8537. (b) Lee, E. P.; Song, S. Y.; Lee, D. W.; Ok, K. M. *Inorg. Chem.* **2013**, *52*, 4097−4103.